

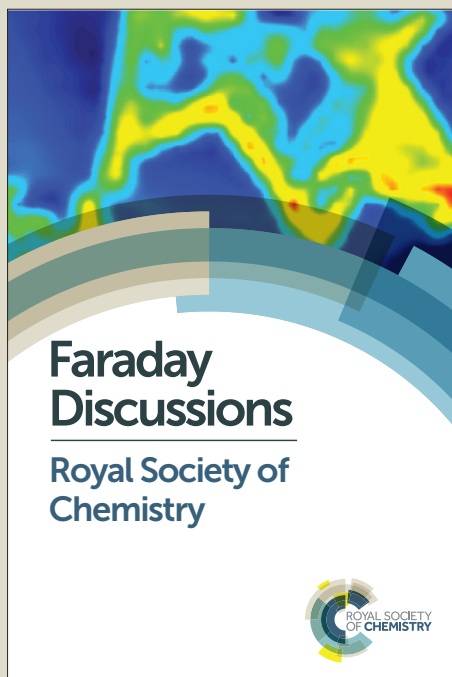
Faraday Discussions

Accepted Manuscript



This manuscript will be presented and discussed at a forthcoming Faraday Discussion meeting. All delegates can contribute to the discussion which will be included in the final volume.

Register now to attend! Full details of all upcoming meetings: <http://rsc.li/fd-upcoming-meetings>



This is an *Accepted Manuscript*, which has been through the Royal Society of Chemistry peer review process and has been accepted for publication.

Accepted Manuscripts are published online shortly after acceptance, before technical editing, formatting and proof reading. Using this free service, authors can make their results available to the community, in citable form, before we publish the edited article. We will replace this *Accepted Manuscript* with the edited and formatted *Advance Article* as soon as it is available.

You can find more information about *Accepted Manuscripts* in the [Information for Authors](#).

Please note that technical editing may introduce minor changes to the text and/or graphics, which may alter content. The journal's standard [Terms & Conditions](#) and the [Ethical guidelines](#) still apply. In no event shall the Royal Society of Chemistry be held responsible for any errors or omissions in this *Accepted Manuscript* or any consequences arising from the use of any information it contains.

Synthesis of mesoporous nanocomposites for their application in solid oxide electrolyser cells: microstructural and electrochemical characterization

M.Torrell, L. Almar, A. Morata, A. Tarancón

*Catalonia Institute for Energy Research (IREC) Jardins de les Dones de Negre, 1, 08930-Sant Adrià de Besòs, Barcelona, Spain; [*atarancon@irec.cat](mailto:atarancon@irec.cat)*

Abstract

Fabrication routes for new SOEC mesoporous nanocomposites materials for electrodes are presented in this paper. NiO-CGO and SDC-SSC are described as possible new materials and their synthesis and the cell fabrication are detailed. The obtained materials are microstructurally characterised by SEM, TEM and XRD, where the mesoporous structures are observed and analysed. Obtained samples are electrochemically analysed by I-V polarisation curves and EIS analysis, showing a maximum current density of 330mA/cm² at 1.7V. A slight drop on the electrolyser performance with the proportion of water in the inlet fuel is detected. A degradation of the cell performance is evidenced after a potentiostatic test at 1.4V during more than 40 hours. Oxygen electrode delaminating is detected, which is most probably the main cause of ageing. Even taking into account the lack of durability of the fabricated cells, the mesoporous electrodes do not seem to be altered, opening the possibility for further studies devoted to this high stable material as SOEC electrodes.

Introduction

The renewable energy sources are nowadays an important piece on the present energy scenario. In 2012, the world relied on renewable sources for around 13% of its total primary energy supply, and in 2013 renewables accounted for almost 22% of global electricity generation, a 5% increase from 2012 ^[1, 2]. These clean energy sources (i.e. solar, wind, geothermal, hydro) present an intrinsic problem of fluctuant production. These fluctuations do not match with the demand of the final consumers and industry. Considering this scenario, the energy storage technology becomes a key factor into the new energy routes to achieve a free or low carbon energy cycle. Unlike battery storage, chemical energy storage represents a relatively low cost alternative with high capacity and long term storage. Water electrolysis technology presents several advantages on the hydrogen production as energy vector and has been shown as the preferred alternatives, the so called power-to-fuel technology. The reasons are the high energy density of hydrogen and the high efficiencies that electrolysis can achieve. This efficiency is especially high when high temperature electrolysers are used to reduce steam to hydrogen, i.e. solid oxide electrolyser cells (SOEC). Low temperature water electrolysers such as alkaline electrolysers or proton exchange membrane are already available in the market. However, these systems present lower efficiencies than SOEC mainly because their higher electrical energy demand and internal resistances. The amount of fuel produced per unit of injected electricity and the hydrogen production rates are remarkably higher in SOECs resulting in more cost-effective hydrogen generation. Moreover, the increase on the operation temperature allows avoiding the use of noble metals as catalyst ^[3, 4]. Nevertheless, the exploitation of these favourable thermodynamics and small resistances of SOECs is up to now hindered by the lack of maturity of this technology. One of the major technical issues is the degradation that the functional materials used in cells electrodes suffer ^[5, 6]. Thermal mismatch ^[7, 8], red-ox cycling ^[9], nickel agglomeration ^[10,11], electrode delamination ^[12] are some of the main problems of durability on solid oxide electrolyser cells. Unlike in the case of SOFC, where decrease the operation temperature has been one of the main objectives of the scientific community to reduce the degradation processes, temperature reduction in

SOEC would promote an undesired effect on the final efficiency due to the increase on the electrical demand of the electrolyser.

It is well-known that some losses associated with the electrode processes can be minimised by engineering the triple phase boundary (TPB). The maximization of the TPB density can promote not only an improvement of the performance but also an improvement of the cell durability. One of the most interesting approaches involves the preparation of interpenetrated nanocomposites showing a high TPB density that avoids the accumulation of the current density in conduction paths ^[13]. The use of nanostructured composites improves different critical aspects of the cells performance. The nanostructured composite electrode ensures a more homogeneous distribution of both phases multiplying the active TPB with two main effects on the electrochemical behaviour of the electrolyser. There are more catalytic active points where the steam reaction can take place and the current density in each point is drastically reduced. In this way the performance and durability of the cell can be improved. Various strategies, such as electrodes impregnation, infiltration and gradual composition of composite electrodes, have been developed to improve the catalytic activity and stability of the SOEC electrodes ^[8, 14-16]. Recent published papers by the authors have been devoted to explore a new family of electrodes based on the infiltration or impregnation of mesoporous scaffolds ^[17-20]. Good performance, thermal stability and, more interestingly, excellent durability under real conditions have been recently published in SOFC operation mode, opening the door for their use in more demanding applications such as high temperature electrolysis.

In this work, the use of nanostructured composites based on mesoporous materials is presented for fuel and oxygen electrodes for solid oxide electrolyser cells (SOEC). Ceramic-metal (cermet) mesoporous composites of Ni-CGO obtained after the reduction of the mesoporous NiO impregnated with CGO were employed as a fuel electrode while Samarium Strontium Cobaltite ($\text{Sm}_{0.5}\text{Sr}_{0.5}\text{CoO}_{3-\delta}$ / SSC) impregnated scaffolds of mesoporous Samarium doped ceria ($\text{Ce}_{0.8}\text{Sm}_{0.2}\text{O}_{1.9}$ / SDC) were used as oxygen electrode. These electrodes were implemented in electrolyte supported cells of $(\text{Sc}_2\text{O}_3)_{0.1}(\text{CeO}_2)_{0.01}(\text{ZrO}_2)_{0.89}$ (ScCeSZ). The mesoporous materials have been

characterised and their synthesis route described. SOEC cells based on mesoporous electrodes were characterized by impedance spectroscopy and in operation conditions under different fuel compositions in order to characterise their performance.

Experimental method

Fabrication of electrolysis cells based on mesoporous electrodes

Solid oxide electrolyser cells based on mesoporous electrodes were fabricated using $(\text{Sc}_2\text{O}_3)_{0.1}(\text{CeO}_2)_{0.01}(\text{ZrO}_2)_{0.89}$ 150 μm commercial tapes (Kerafold) as an electrolyte. Scandia and ceria-doped zirconia electrolytes were used to achieve better performances of the electrolyser at temperatures below 900°C. The use of multi valence cations, i.e. cerium, as dopant of the zirconia electrolyte has been proposed as a solution to avoid oxygen electrode interphase degradation ^[12]. A diffusion barrier of 2 μm of $\text{Ce}_{0.8}\text{Gd}_{0.2}\text{O}_{1.9}$ (CGO) was deposited between the oxygen electrode and the electrolyte by Pulsed Laser Deposition (PLD) to prevent the formation of insulating phases observed when zirconia is in contact with La- and/or Sr-based cathodes ^[21-24].

Mesoporous powders of a cermet of nickel and gadolinium doped ceria were synthesized to fabricate the fuel electrode of the SOEC electrolyser. Impregnation of powder of silica KIT-6 with *Ia3d* symmetry was carried out by using Ni precursor of $(\text{Ni}(\text{NO}_3)_2 \cdot 6\text{H}_2\text{O})$ in ethanol solution and annealed at 600°C-5h to obtain the NiO crystalline desired mesoporous phase. Afterwards, the silica template was removed by employing a solution of NaOH 2M at 70°C. A detailed description of the whole process can be found elsewhere ^[17]. Obtained NiO replicas were impregnated with cerium nitrate and gadolinium nitrate salts with the stoichiometry necessary to obtain the $\text{Ce}_{0.9}\text{Gd}_{0.2}\text{O}_2$ (CGO) and crystallize inside the NiO mesoporous structure at $T=1100^\circ\text{C}$ -3h. The final obtained powder corresponds to a mesoporous interpenetrated structure of NiO:CGO (50:50 wt%). An ethanol based ink for airbrushing was prepared to deposit the fuel electrode. 30 μm thick NiO-CGO layers were airbrushed onto the ScCeSZ surface and attached by an annealing treatment at 1200°C-3h. A commercial nickel ink (Fuel-Cell materials) layer was painted and attached at 900°C-1h above the electrode to improve the current collection of the electrode.

Mesoporous powder of samarium doped cerium (SDC) were synthesised and attached to the CGO barrier layer. Mesoporous SDC was fabricated from KIT-6 hard template which was impregnated in an ethanol solution of the SDC precursors and annealed at 600°C -5 h. The silica template was removed by NaOH 2M solution cleaning process. The so-obtained powder was used to prepare an ethanol-based airbrushing ink to deposit 15 µm thick layers of porous SDC scaffold onto the CGO barrier deposited by PLD. The attachment was carried out at 1000°C during 3h in air. After the attachment step, the SDC was functionalized as catalytic cathode by infiltration of samarium strontium cobaltite (SSC). SDC was impregnated with stoichiometric amounts of $\text{Sm}(\text{NO}_3)_3$, $\text{Sr}(\text{NO}_3)_2$, $\text{Co}(\text{NO}_3)_2 \cdot 6\text{H}_2\text{O}$ previously mixed in a water and ethanol solution of 0.1M. Three impregnation steps of 20 µL of solution were carried out in order to ensure a good infiltration followed by a final annealing treatment at 800°C for 2h. SSC commercial ink layers were finally painted and attached at 900°C for 1h.

Microstructural and electrochemical characterisation

The electrodes were micro structurally characterised by Zeiss Auriga scanning electron microscope (SEM). X-Ray diffraction studies were performed in a Bruker D8 Advance diffractometer in 2θ reflection mode from 20 to 80° using a copper $\text{K}_{\alpha 1}$ radiation. The electrochemical and fuel cell tests were carried out in a commercial ProboStat™ (NorEcs AS) sample holder placed inside a high temperature tubular furnace. A galvanostat/potentiostat with EIS capabilities (Parstat 2273, PAR) was employed for the electrochemical measurements. A frequency range from mHz to MHz was covered by applying ac voltages of 50 mV over OCV or operation voltages (1.4V). The test station allows a compositional control of the water content in the fuel gas inlet mixture. Ultrapure water is evaporated by a controlled evaporator and mixing liquid delivery system (Bronkhorst–CEM system) that regulates and monitors the steam flow by a liquid flow controller.

Results

Structural characterisation of SOEC electrodes

Mesoporous NiO was microstructurally characterised by SEM after the nanocasting synthesis process. Figure 1a shows the powder microstructure, which is a direct replica of the mesoporous structure of the original hard template of KIT-6. The NiO powder presents nanoscaled porosity with periodicity and homogeneity throughout the observed powder. Low angle transmission XRD (not shown here) was also carried out to ensure the mesoporosity of the prepared powder. The XRD pattern presented in Figure 1b corroborates the crystallization of CGO after impregnation of the NiO scaffold. The intimate interpenetration of the two phases was analyzed by the authors by TEM-EELS in a previous publication ^[18]. The SEM cross section image presented in the Figure 1c shows a 12 μm thick homogeneous and uniform porous electrode after the attachment of the interpenetrated NiO-CGO to the electrolyte at 1200°C-3h.

Mesoporous SDC employed as scaffold for the oxygen electrode was also characterised by SEM after the nanocasting synthesis based on KIT-6 hard template and the subsequent KIT-6 removal step. The SEM micrograph of the Figure 2a shows the mesoporous structure of the as-synthesized SDC powder. It can be clearly appreciated the mesoporous structure of the grains and the periodicity of the pores. The XRD pattern presented in the Figure 2b was acquired after the crystallization step of the SSC-SDC nanocomposite and confirms the formation of both compounds. A diffraction peak corresponding to a parasitic phase can be observed at $2\theta=37^\circ$. This was attributed to Co_3O_4 and it is not expected to significantly affect the final performance of the electrode. Figure 2c shows the SEM cross section of the SDC-SSC layer after being attached to the CGO diffusion barrier. A uniform and porous layer of 18 μm in thickness is observed. The 2 μm thick PLD diffusion layer can also be clearly appreciated. The use of a dense and continuous layer of CGO avoids the formation of insulating layers at the operation temperatures.

Electrochemical testing

Mesoporous based electrolyser cells were electrochemically characterised through EIS and their performance evaluated by acquisition of I-V polarization curves when operating under three different fuel compositions at 850°C. The used fuel compositions were balanced with Argon, obtaining the following compositions: (i) 14% H_2O -72 % H_2 -

14%Ar, (ii) 25% H_2O -62.5% H_2 -12.5%Ar and (iii) 40% H_2O -50% H_2 -10%Ar. Figure 3 shows the injected current density as a function of the voltage and for the different fuels under study. No significant differences were observed on the solid oxide cell electrolyser performance with the different fuel compositions indicating a certain fuel flexibility of the SOEC. An open circuit voltage (OCV) of 0.94V demonstrates gas tight chambers for the oxygen and the fuel. At 1.7V, a maximum value of injected current of 330mA/cm² was reached. This injected current density compares well with previously reported values for SOECs [25-29]. M. Laguna-Bercero et al. reported about 400mA/cm² at 1.7V with 80% H_2O using Ni-YSZ/ScCeSZ/Pt cells at 800°C with ASR of 1.22 $\Omega\cdot\text{cm}^2$ [26]. Basile et al. present for 50% H_2O at 800°C current densities below 300mA/cm² at 1.5V [27]. At temperatures higher than 900°C, X. Yue and J.T.S. Irvine injected more than 900 mA/cm² at voltages below 1V in a LSCM-CGO/YSZ/LSM with only 3% H_2O [25]. The authors recently published a symmetric cell where 650mA/cm² were injected at 850°C and 1.6V [30]. The linear shape of the I-V curve does not evidence any gas diffusion problem or electrode high activation barrier.

A more detailed study of the different contributions to the total resistance of the cells was carried out by the Electrochemical Impedance Spectroscopy (EIS). Figure 4 shows the Nyquist plots corresponding to the EIS measurements carried out at OCV and 1.4V. The spectra can be adjusted by employing a simple $R_s(R_1Q_1)(R_2Q_2)$ equivalent circuit. More than half of the total resistance is associated to in series contributions (Figure 4a). This high resistance was ascribed to an insufficient adhesion between the electrolyte and the electrodes (the electrolyte itself showed a low resistance for independent measures). The high thermal stability of the mesoporous SDC previously demonstrated by the authors [18] could be in the origin of this phenomenon. In order to focus the analysis on the resistance strictly associated to the electrode performance, deconvoluted versions of the spectra were included in Figure 4b and 4c for OCV and 1.4V. Similar polarization resistances with area specific resistance (ASR) below 1 Ωcm^2 were observed for the different fuel compositions under study [25-30]. Although the remarkable values, a better performance is expected after overcoming adhesion issues previously mentioned. Further work is ongoing to reach a reasonable trade off in terms of attachment temperature to ensure a proper adhesion while maintaining the

mesoporous nature of the electrodes. Another possible cause of the low performance could be the SiO_2 contain remaining from the KIT-6 template after the alkaline washing step, and its negative effect on the electrode performance. Si content was evaluated by EDX after 4 alkaline washing steps at 70°C with NaOH 2M, followed by 3 washing steps with deionised pure water and was presented elsewhere ^[19]. The percentage of remaining Si is reduced to 1.16 wt%. This value is above the level of impurities of Si in commercial CGO (< 100 ppm), but at the same time the high surface area minimise the proportion of blocked surface in the mesoporous.

Mid-term test of the SOEC

The SOEC cell was also tested during 40h at 1.4V in potentiostatic mode when subjected to an atmosphere of 25% H_2O -62.5% H_2 -12,5% Ar at 850°C. The evolution of the I-V polarisation curves with the operation time can be observed in the Figure 5. A significant drop of the electrolyser performance takes place during the first 25 hours of operation. The increase of the resistance shown in the slope change of the I-V curves is corroborated with the continuous evolution of the current during the potentiostatic test (insert on figure 5). The current density during the potentiostatic test decreases from the initial 150 mA/cm² to the final 110 mA/cm² after 40 hours of test.

Impedance spectra were acquired at the operation voltage of 1.4V at different times during the experiment. Corresponding Nyquist plots are presented in Figure 6. Similar spectra shapes are observed with time. Accordingly, the equivalent circuit employed before was used for deconvolution of the whole range of data. The values obtained by fitting with the equivalent circuit elements have been summarised on the table I. As previously mentioned, ohmic contribution represents a significant amount of the total resistance. Moreover, this contribution continuously increases with the operation time from the initial 1.17 $\Omega\cdot\text{cm}^2$ to the final 1.71 $\Omega\cdot\text{cm}^2$. This clearly indicates a progressive delamination of the electrodes (probably due to the weakness suggested in the preceding section). The ASR associated to the electrode is correspondingly increasing from 0.74 $\Omega\cdot\text{cm}^2$ to 1.35 after 41 hours of test.

In order to confirm the source of this degradation, a post mortem structural characterization was carried out. Microstructures of the fuel and oxygen electrodes after the mid-term test are shown on figures 7 and 8, respectively. While the internal microstructure of the electrodes was preserved, an evident degradation of the oxygen electrode/CGO-layer interface is present when compared with figure 2c. Therefore, the origin of this delamination will be likely associated to previously reported issues observed in the oxygen electrode. This behaviour was described by Virkar ^[12] as a consequence of the increase of the internal oxygen pressure within the diffusion barrier and oxygen electrode. These degradation has been already described on solid oxide electrolyzers by different authors ^[31, 32]. Once the contact points between electrode and

electrolyte are affected, the electrode performance decreased as well as the actual active area decreases. Graves et al. recently proposed the reversible alternative use in SOFC-SOEC mode of the cell showing important improvements on the cell degradation resistance ^[32].

Conclusions

Mesoporous nanocomposite electrodes have been presented as a novel material for electrode in solid oxide electrolyser cells. Mesoporous nanocomposite electrodes of NiO-CGO mesoporous cermet have been synthesised by wet impregnation route and deposited in ScCeSZ electrolyte as a fuel electrode and their fabrication described. SDC-SSC mesoporous nanocomposite has been obtained by infiltration of the scaffold attached to the electrolyte and used as oxygen electrode. The maximum value of current density injected at 1.7V was of 330 mA/cm² at a temperature of 850°C. A significant ohmic resistance was observed for all the fabricated cells. This is probably due an insufficient adhesion of the electrode to the electrolyte caused by the high thermal stability of the mesoporous materials previously shown by the authors. The optimisation of the electrode attachment temperatures seems to be a crucial factor especially when highly thermal stable materials like this are used. Therefore, although the high stability of the mesoporous materials has a great potential to reduce degradation of SOEC electrodes, further work is required to ensure the good adhesion required to take advantage of this.

Acknowledgements

The authors want to acknowledge MINECO for the CHISTE project (ENE2013-47826-C4-3-R) that funded the acquisition of presented results.

References

- ¹ Ni, M., Leung, M., Leung, D. Technological development of hydrogen production by solid oxide electrolyzer cell (SOEC). *Int. J. Hydrogen Energy* **33**, 2337–2354 (2008), 131–135 (2012).
- ² <http://www.iea.org/aboutus/faqs/renewableenergy/>
- ³ Nechache, A., Cassir, M. & Ringuedé, A. Solid oxide electrolysis cell analysis by means of electrochemical impedance spectroscopy: A review. *J. Power Sources* **258**, 164–181 (2014).
- ⁴ Tarancón, A., Fábrega, C., Morata, A., Torrell, M., Andreu, T.. Materials for Energy, Chapter: Power to fuel and artificial photosynthesis for chemical energy storage. Ed. D. Muñoz, X. Moya. Pan Stanford Publishing. 2015.
- ⁵ Wang, K. *et al.* A Review on solid oxide fuel cell models. *Int. J. Hydrogen Energy* **36**, 7212–7228 (2011).
- ⁶ Yokokawa, H., Tu, H., Iwanschitz, B. & Mai, A. Fundamental mechanisms limiting solid oxide fuel cell durability. *J. Power Sources* **182**, 400–412 (2008).
- ⁷ Howe, K. S. *et al.* Performance of microtubular SOFCs with infiltrated electrodes under thermal cycling. *Int. J. Hydrogen Energy* **38**, 1058–1067 (2013).
- ⁸ Jiang, S. P. Nanoscale and nano-structured electrodes of solid oxide fuel cells by infiltration: Advances and challenges. *Int. J. Hydrogen Energy* **37**, 449–470 (2012).
- ⁹ Faes, A., Hessler-Wyser, A., Zryd, A. & Van herle, J. A Review of RedOx Cycling of Solid Oxide Fuel Cells Anode. *Membranes (Basel)*. **2**, 585–664 (2012).
- ¹⁰ Iwanschitz, B., Holzer, L., Mai, A. & Schütze, M. Nickel agglomeration in solid oxide fuel cells: The influence of temperature. *Solid State Ionics* **211**, 69–73 (2012).
- ¹¹ Simwonis, D. Nickel coarsening in annealed Ni/8YSZ anode substrates for solid oxide fuel cells. *Solid State Ionics* **132**, 241–251 (2000).
- ¹² Virkar, A. V. Mechanism of oxygen electrode delamination in solid oxide electrolyzer cells. *Int. J. Hydrogen Energy* **35**, 9527–9543 (2010).
- ¹³ Jiang, S. P. Nanoscale and nano-structured electrodes of solid oxide fuel cells by infiltration: Advances and challenges. *Int. J. Hydrogen Energy* **37**, 449–470 (2012).
- ¹⁴ Murray, E. P., Tsai, T. & Barnett, S. A. Oxygen transfer processes in (La,Sr)MnO₃/Y₂O₃-stabilized ZrO₂ cathodes: an impedance spectroscopy study. *Solid State Ionics* **110**, 235–243 (1998).
- ¹⁵ Park, Y. M., Kim, J. H. & Kim, H. High-Performance composite cathodes for solid oxide fuel cells. *Int. J. Hydrogen Energy* **36**, 9169–9179 (2011).
- ¹⁶ Matsuzaki, Y. Electrochemical properties of a SOFC cathode in contact with a chromium-containing alloy separator. *Solid State Ionics* **132**, 271–278 (2000).
- ¹⁷ Almar, L. *et al.* High-surface-area ordered mesoporous oxides for continuous operation in high temperature energy applications. *J. Mater. Chem. A* **2**, 3134 (2014).
- ¹⁸ Almar, L. *et al.* High-Temperature Long-Term Stable Ordered Mesoporous Ni-CGO as an Anode for Solid Oxide Fuel Cells. doi:10.1039/b000000x

-
- ¹⁹ Almar, L., Andreu, T., Morata, A. & Tarancón, A. Mesoporous NiO-CGO Obtained by Hard Template as High Surface Area Anode for IT-SOFC. in *ECS Trans.* **35**, 1647–1654 (2011).
- ²⁰ Almar, L., Morata, A., Torrell, M., Gong, M., Liu, M., Andreu, T., Tarancon, A. “Synthesis and characterisation of robust, mesoporous electrodes for solid oxide fuel cell”. *Nanoenergy* (Submitted 2015).
- ²¹ Knibbe, J. Hjelm, M. Menon, N. Pryds, M. Søgaard, H. J. Wang and K. Neufeld, *J. Am. Ceram. Soc.*, 2010, **93**, 2877–2883.
- ²² Choi, M.-B., Singh, B., Wachsman, E. D. & Song, S.-J. Performance of La_{0.1}Sr_{0.9}Co_{0.8}Fe_{0.2}O_{3-δ} and La_{0.1}Sr_{0.9}Co_{0.8}Fe_{0.2}O_{3-δ}-Ce_{0.9}Gd_{0.1}O₂ oxygen electrodes with Ce_{0.9}Gd_{0.1}O₂ barrier layer in reversible solid oxide fuel cells. *J. Power Sources* **239**, 361–373 (2013).
- ²³ Hjalmarsson, P., Sun, X., Liu, Y.-L. & Chen, M. Influence of the oxygen electrode and inter-diffusion barrier on the degradation of solid oxide electrolysis cells. *J. Power Sources* **223**, 349–357 (2013).
- ²⁴ Klemensø, T., Nielsen, J., Blennow, P., Persson, A. H., Stegk, T., Christensen, B. H. & Sønderby, S., *J. Power Sources*, 2011, **196**, 9459–9466.
- ²⁵ Yue, X., Irvine, J. T. S. (La,Sr)(Cr,Mn)O₃/GDC cathode for high temperature steam electrolysis and steam-carbon dioxide co-electrolysis. *Solid State Ionics* **225**
- ²⁶ Laguna-Bercero, M. A., Skinner, S. J. & Kilner, J. A. Performance of solid oxide electrolysis cells based on scandia stabilised zirconia. *CONAPPICE 2008*, Zaragoza, Spain, 24-26 Sept. 2008 **192**, 126–131 (2009)
- ²⁷ Basile, A. et al. Gadolinium doped ceria-impregnated nickel–yttria stabilised zirconia cathode for solid oxide electrolysis cell. *Int. J. Hydrogen Energy* **36**, 9420–9427 (2011).
- ²⁸ Liu, Q., Yang, C., Dong, X. & Chen, F. Perovskite Sr₂Fe_{1.5}Mo_{0.5}O_{6-δ} as electrode materials for symmetrical solid oxide electrolysis cells. *Int. J. Hydrogen Energy* **35**, 10039–10044 (2010).
- ²⁹ Hjalmarsson, P., Sun, X., Liu, Y.-L. & Chen, M. Influence of the oxygen electrode and inter-diffusion barrier on the degradation of solid oxide electrolysis cells. *J. Power Sources* **223**, 349–357 (2013).
- ³⁰ Torrell, M., García-Rodríguez, S., Morata, A., Penelas, G., Tarancon, A., Co-electrolysis of steam and CO₂ in full-ceramic symmetrical SOECs: A strategy for avoiding the use of Hydrogen as a safe gas. *Faraday Discussions*. 2015 DOI: 10.1039/C5FD00018A.
- ³¹ Li, S., Li, Y., Gan, Y., Xie, K. & Meng, G. Electrolysis of H₂O and CO₂ in an oxygen-ion conducting solid oxide electrolyzer with a La_{0.2}Sr_{0.8}TiO_{3+δ} composite cathode. *J. Power Sources* **218**, 244–249 (2012).
- ³² Graves, C., Ebbesen, S. D., Jensen, S. H., Simonsen, S. B. & Mogensen, M. B. Eliminating degradation in solid oxide electrochemical cells by reversible operation. *Nat. Mater.* (2014). doi:10.1038/nmat4165

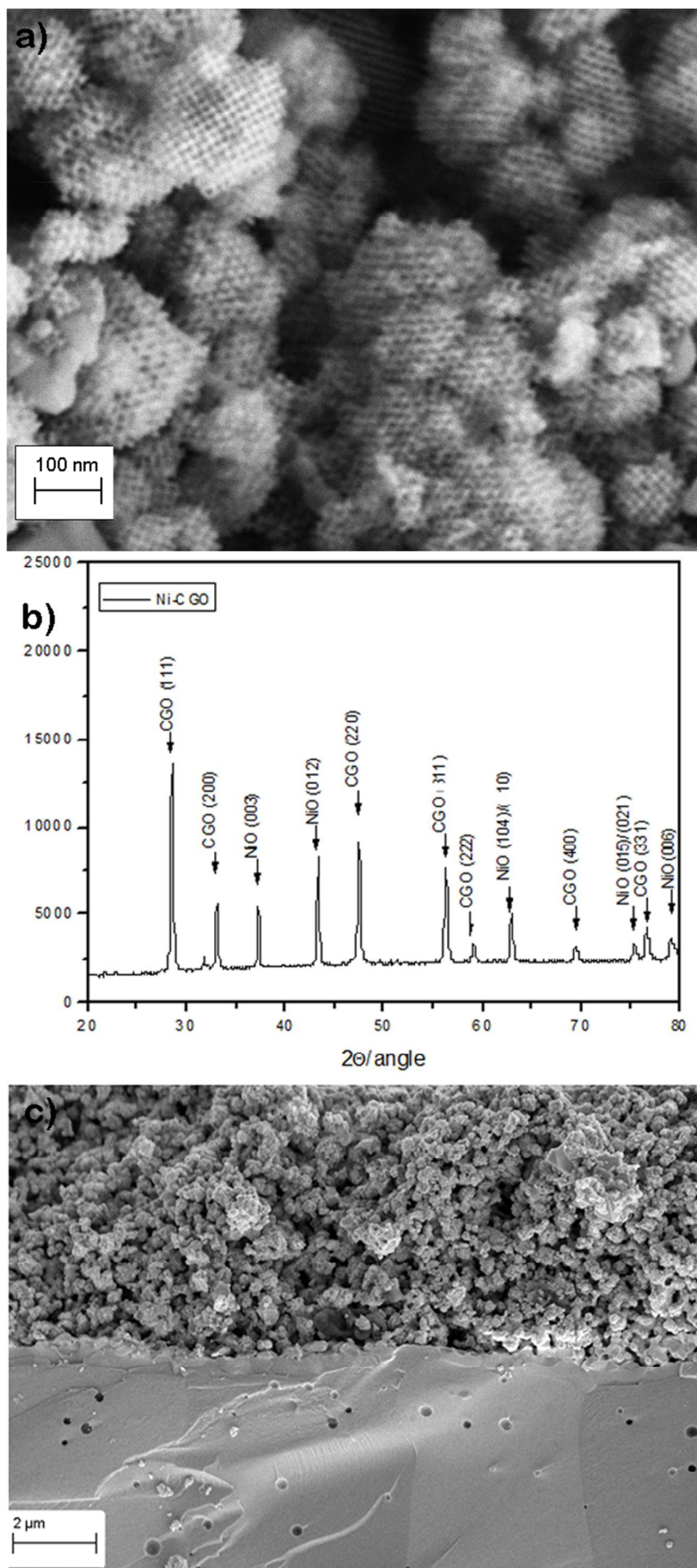


Fig.1 a) SEM images of the mesoporous NiO powder as synthesised. b) XRD pattern of the NiO after the CGO impregnation and calcination. c) NiO-CGO mesoporous nanocomposite attached to the ScCeSZ electrolyte at 1200°C.

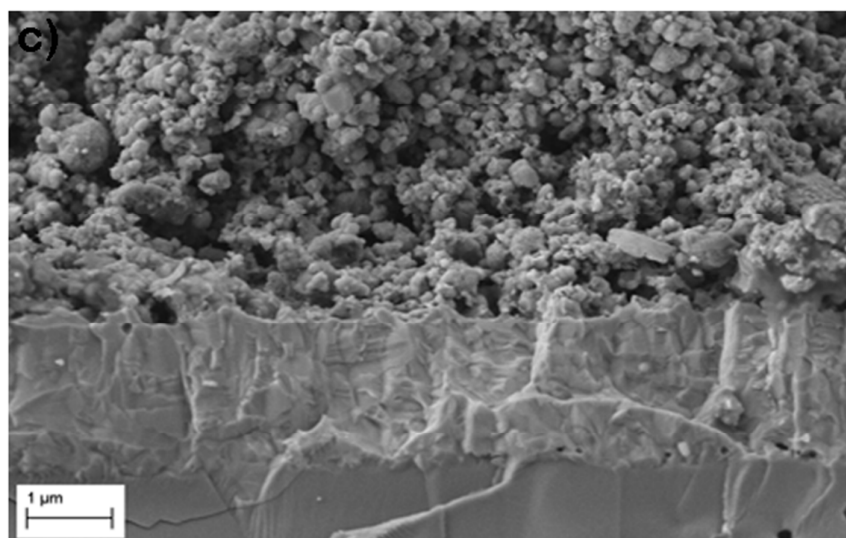
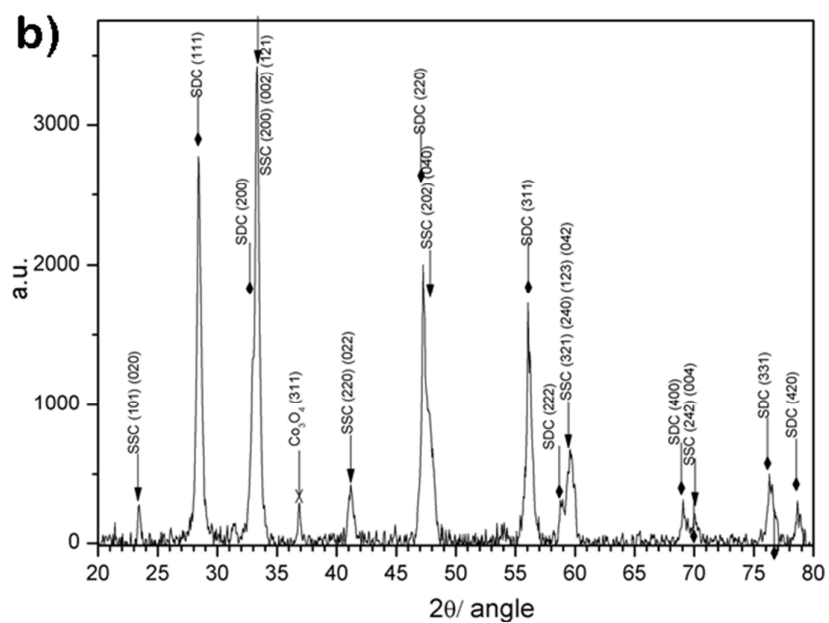
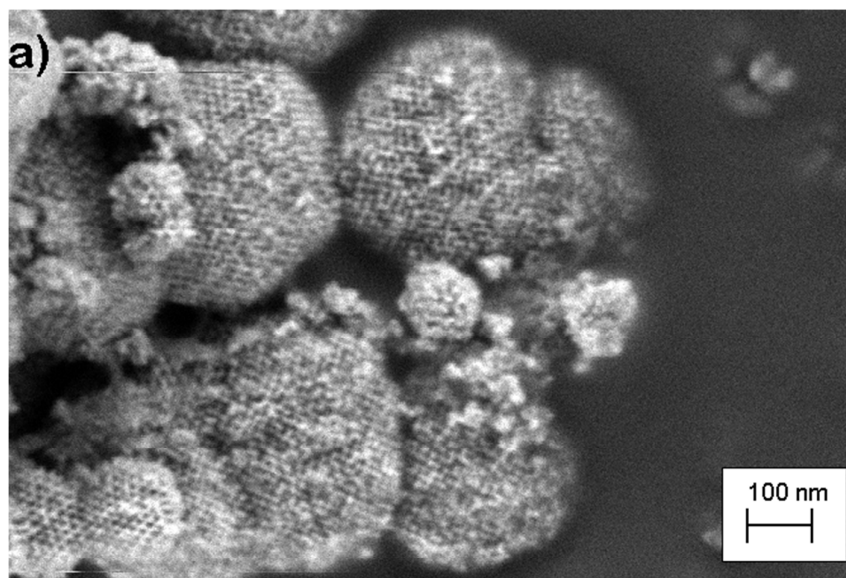


Fig 2 a) SEM images of the SDC powder before to attach to the electrolyte as a ceramic scaffold for its infiltration with SSC. b) XRD pattern of the SDC-SSC composite. c) SDC-SSC infiltrated mesoporous layer attached to the CGO diffusion barrier growth over the ScCeSZ electrolyte.

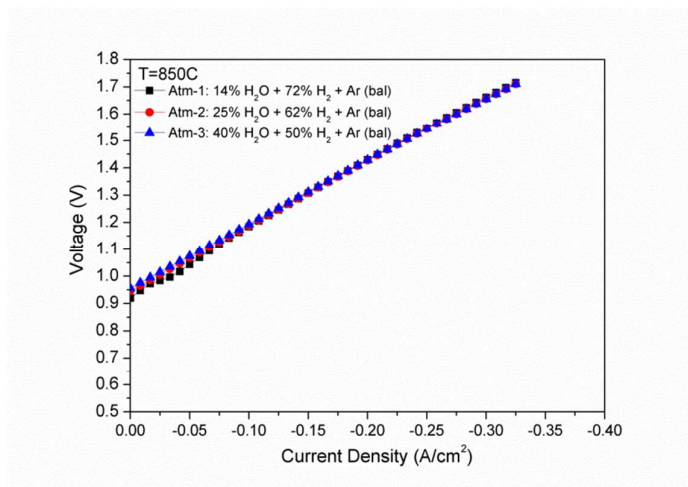


Fig. 3 I-V polarization curves at different fuel compositions obtained at 850°C.

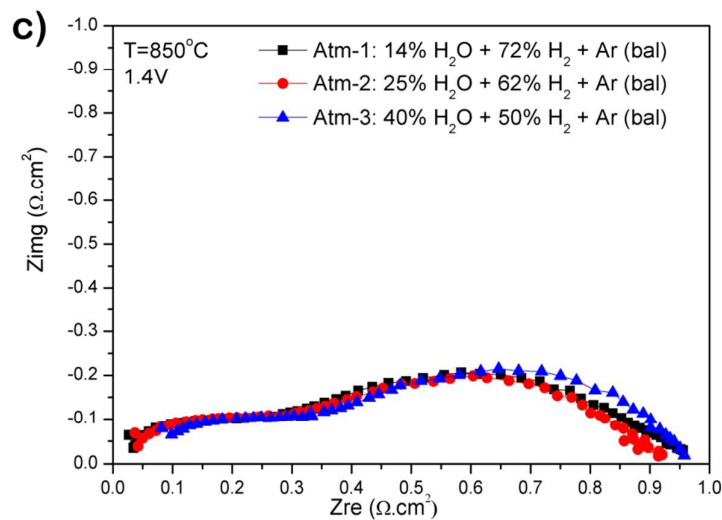
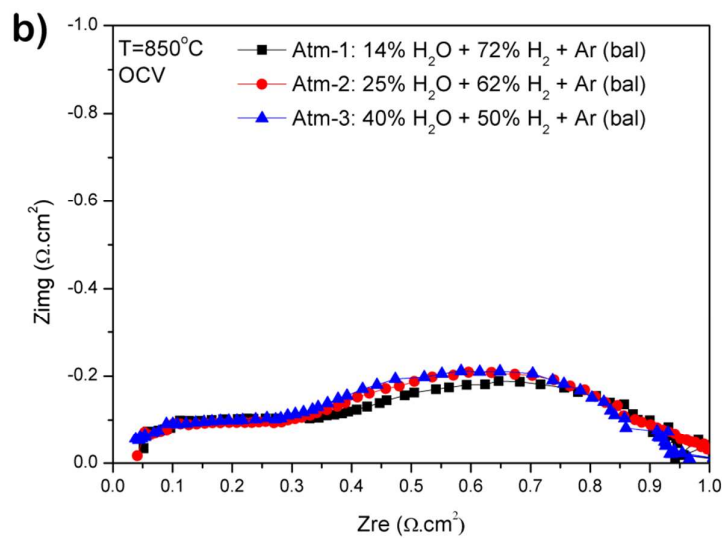
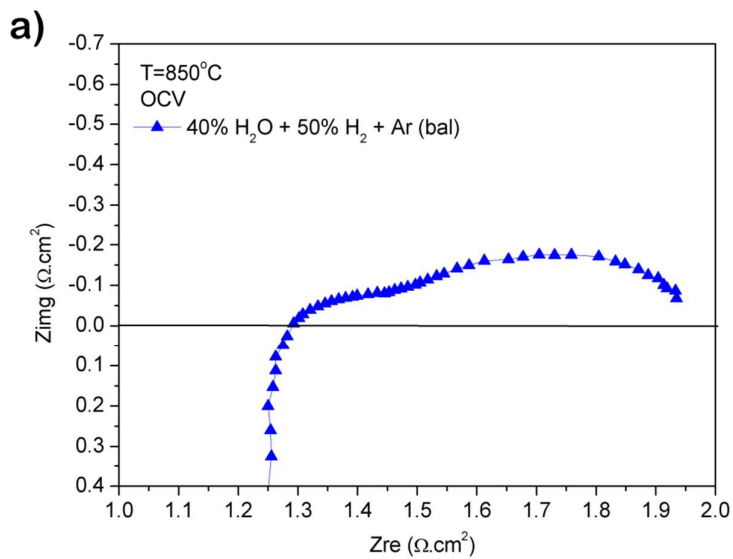


Fig. 4 a) Complete Nyquist diagram of the EIS obtained at 40% of H₂O and 50% of H₂ (Ar bal.) operating at 850°C b) and c) OCV and 1.4V at different fuel compositions where inductance and ohmic resistance have been subtracted.

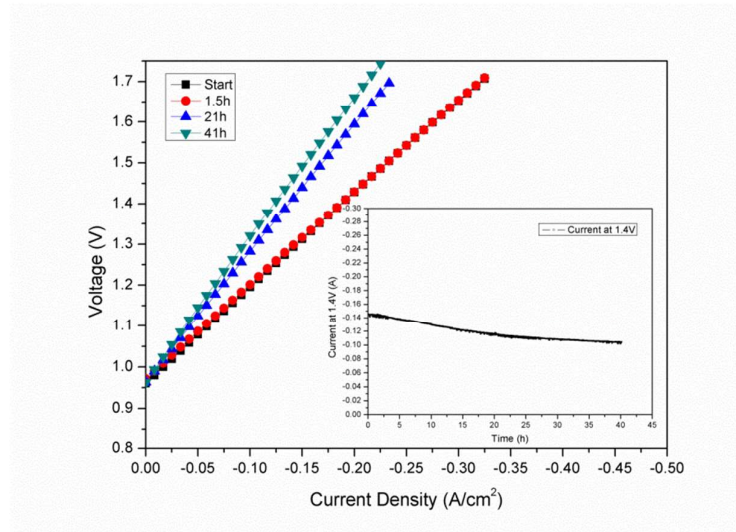


Fig. 5 Evolution of the mesoporous based electrolyser during the first 40 hours and studied by the evolution of the I-V curves and potentiostatic test (inset of the figure).

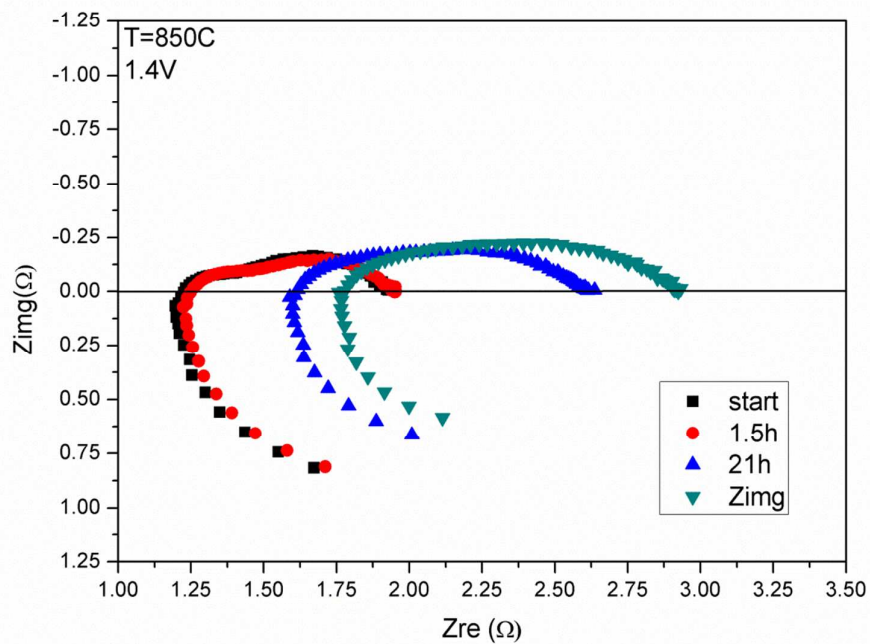


Fig 6. Nyquist plots at 1.4V measured at different operation times of the aging tests

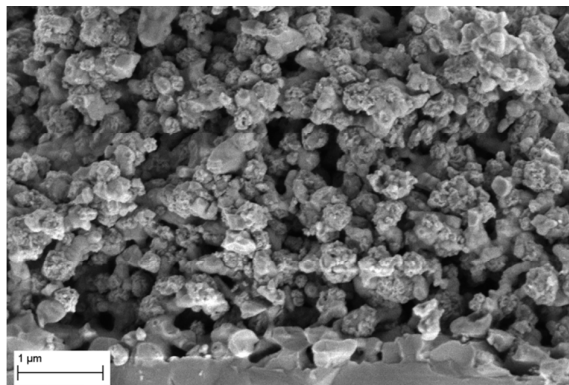


Fig. 7 SE-SEM cross section images of the Ni-CGO fuel electrode after the aging test during 41 hours.

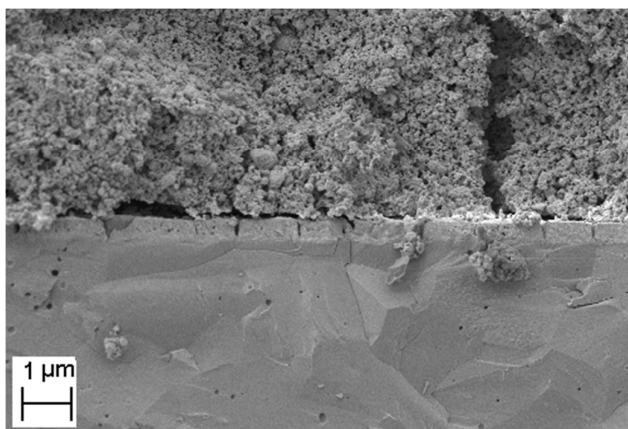


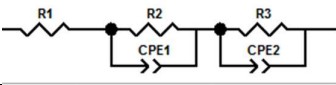
Fig. 8 SE-SEM cross section images of the SDC-SSC oxygen electrode after the aging test during 41 hours.

TABLES

Table I Summary of the obtained resistance contributions by equivalent circuit fitting of the Nyquist diagrams of EIS.

	Start ($\Omega \cdot \text{cm}^2$)	1.5 h ($\Omega \cdot \text{cm}^2$)	20 h ($\Omega \cdot \text{cm}^2$)	41h ($\Omega \cdot \text{cm}^2$)	ΔR ($\Omega \cdot \text{cm}^2$)
Ohmic resistance (R_1)	1.17	1.21	1.56	1.71	0.54
Polarization resistance (R_2, R_3)	0.74	0.72	1.30	1.35	0.61

Table I Summary of the obtained resistance contributions by equivalent circuit fitting of the Nyquist diagrams of EIS.

	Start ($\Omega \cdot \text{cm}^2$)	1.5 h ($\Omega \cdot \text{cm}^2$)	20 h ($\Omega \cdot \text{cm}^2$)	41h ($\Omega \cdot \text{cm}^2$)	ΔR ($\Omega \cdot \text{cm}^2$)
Ohmic resistance (R_1)	1.17	1.21	1.56	1.71	0.54
Polarisation resistance (R_2+R_3)	0.74	0.72	1.30	1.35	0.61